PHYSICAL REVIEW B **95**, 241105(R) (2017)

$MoTe_2$: An uncompensated semimetal with extremely large magnetoresistance

S. Thirupathaiah,[1,*] Rajveer Jha,[2] Banabir Pal,[1] J. S. Matias,[2] P. Kumar Das,[3,4] P. K. Sivakumar,[1] I. Vobornik,[3] N. C. Plumb,[5] M. Shi,[5] R. A. Ribeiro,[2] and D. D. Sarma[1]

[1]*Solid State and Structural Chemistry Unit, Indian Institute of Science, Bangalore, Karnataka 560012, India*
[2]*CCNH, Universidade Federal do ABC (UFABC), Santo Andre, SP 09210-580 Brazil*
[3]*CNR-IOM, TASC Laboratory AREA Science Park-Basovizza, 34149 Trieste, Italy*
[4]*International Centre for Theoretical Physics, Strada Costiera 11, 34100 Trieste, Italy*
[5]*Paul Scherrer Institut, Swiss Light Source, CH-5232 Villigen PSI, Switzerland*

(Received 2 February 2017; published 8 June 2017)

Transition-metal dichalcogenides (WTe_2 and $MoTe_2$) have recently drawn much attention, because of the nonsaturating extremely large magnetoresistance (XMR) observed in these compounds in addition to the predictions of likely type-II Weyl semimetals. Contrary to the topological insulators or Dirac semimetals where XMR is linearly dependent on the field, in WTe_2 and $MoTe_2$ the XMR is nonlinearly dependent on the field, suggesting an entirely different mechanism. Electron-hole compensation has been proposed as a mechanism of this nonsaturating XMR in WTe_2, while it is yet to be clear in the case of $MoTe_2$ which has an identical crystal structure of WTe_2 at low temperatures. In this Rapid Communication, we report low-energy electronic structure and Fermi surface topology of $MoTe_2$ using angle-resolved photoemission spectrometry (ARPES) technique and first-principles calculations, and compare them with that of WTe_2 to understand the mechanism of XMR. Our measurements demonstrate that $MoTe_2$ is an uncompensated semimetal, contrary to WTe_2 in which compensated electron-hole pockets have been identified, ruling out the applicability of charge compensation theory for the nonsaturating XMR in $MoTe_2$. In this context, we also discuss the applicability of other existing conjectures on the XMR of these compounds.

DOI: 10.1103/PhysRevB.95.241105

Materials showing extremely large magnetoresistance (XMR) have potential applications in spintronics. Among them, the semimetals, WTe_2 and $MoTe_2$, have recently attracted a great deal of research interest as they show nonsaturating extremely large MR [1,2] even at 60 T of applied field in addition to the prediction of Weyl nodes [3,4]. While a negative MR is widely known in many magnetic materials [5–7], positive MR has been noticed in some nonmagnetic materials [8–11]. Some of these nonmagnetic compounds such as $Ag_{2+\delta}Te/Se$ [9,11], graphene [12], Bi_2Te_3 [13,14], and Cd_3As_2 [15,16] show linearly field-dependent MR, while type-II Weyl semimetals (WTe_2 and $MoTe_2$) [1,2], LaSb [17], and ZrSiS [18] show quadratic dependence of MR on the field.

Charge compensation is explained as a mechanism of nonsaturating XMR in the compounds showing quadratic field-dependent MR, while nontrivial band topology is thought to be responsible for the same in compounds showing linear field-dependent MR. An angle-resolved photoemission spectrometry (ARPES) report on WTe_2 demonstrated temperature-dependent band structure that is consistent with the temperature-dependent MR [19], thus supporting the conjecture of the charge compensation [1], while the other ARPES reports point to the importance of the spin-orbit coupling and the impact of the thickness dependence of the charge compensation [20,21]. An ARPES report on LaSb showed temperature-independent band structure, while MR is still temperature dependent [17]. Interestingly, a recent ARPES report on YSb has pointed out that these two mechanisms could not explain the observed XMR in YSb which is neither a topological semimetal nor a Weyl semimetal [22]. All of these experimental observations are clearly demonstrating that there is no consensus yet on the mechanism of XMR in the nonmagnetic semimetals.

In this Rapid Communication, we report the electronic structure of $MoTe_2$ using high-resolution angle-resolved photoemission spectroscopy and first-principles calculations. Although there exist few ARPES reports on $MoTe_2$ [23–29], discussing mostly the predictions of Weyl nodes, no ARPES report has addressed the origin of XMR in $MoTe_2$ to date. Here, we show that although the low temperature crystal structure of both $MoTe_2$ and WTe_2 is identical, the bulk electronic structure of $MoTe_2$ is markedly different from WTe_2. We found three interconnected hole pockets and four disconnected electron pockets in $MoTe_2$ in our ARPES studies which are qualitatively supported by our density functional theory (DFT) calculations. Previous ARPES reports on $MoTe_2$ showed electron pockets that are located only along the Γ-X direction. In our ARPES measurements and DFT calculations we realized another pair of electron pockets located at each of the Y points. We further noticed temperature-independent band structure when measured between 20 and 130 K. As the net size of hole pockets is larger than that of the net size of electron pockets in addition to the temperature-independent band structure, the conjecture of charge compensation appears to be invalid for $MoTe_2$ in explaining the property of nonsaturating XMR. Thus, our electronic structure studies of $MoTe_2$ rule out the mechanism of charge compensation as a cause of the unsaturated XMR in these compounds.

Good quality single crystals of stoichiometric $MoTe_2$ were grown using self-flux at Universidade Federal do ABC, Brazil as discussed in Ref. [2]. The crystals have a plateletlike shape with a shiny surface. The crystals were structurally characterized using powder x-ray diffraction to confirm the bulk

*t.setti@sscu.iisc.ernet.in

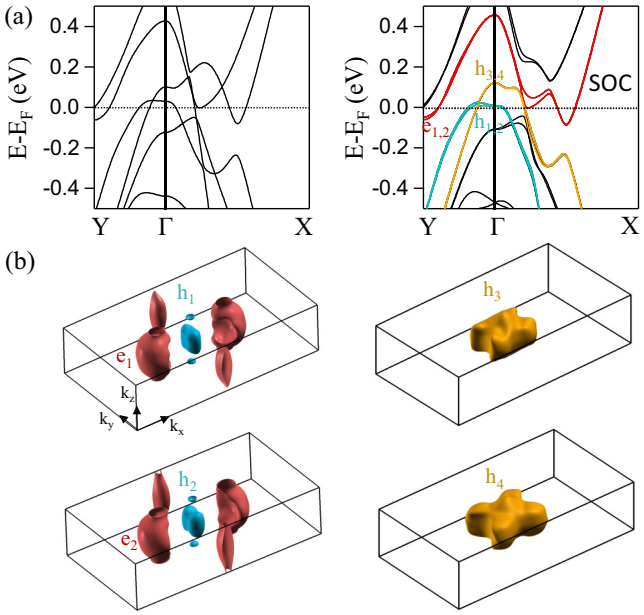

FIG. 1. (a) Calculated band structure of $MoTe_2$ without (left panel) and with spin-orbit coupling (right panel). (b) Three-dimensional view of the calculated Fermi surfaces with spin-orbit coupling. See Ref. [31] for details on the first-principles calculations.

purity and the monoclinic crystal structure with the $P2_1/m1$ space group [see Fig. S1(b) in the Supplemental Material [30]]. ARPES measurements were performed in Swiss Light Source at the SIS beamline using a VG-Scienta R4000 electron analyzer and at the APE beamline in Elettra Synchrotron, Trieste equipped with a Scienta DA30 deflection analyzer. The angular resolution was set at 0.2° for R4000 and at 0.3° for DA30. The used photon energy ranged between 20 and 45 eV. The overall energy resolution was set between 15 and 25 meV depending on the photon energy and beamline employed. Samples were cleaved *in situ* at a temperature of 20 K and the chamber vacuum was better than 5×10^{-11} mbar during the measurements. ARPES measurements were performed on two samples broken from a single big crystal, named here as A and B to differentiate from each.

In the energy-momentum ($E-k$) plot [see left panel in Fig. 1(a)] obtained from the DFT calculations without spin-orbit interaction we identify two holelike bands dispersing along the Γ-X and Γ-Y directions, while an electronlike band disperses along the Γ-Y direction and another electronlike band disperses along the Γ-X direction. It is interesting to see from Fig. 1(a) that one of the hole bands shows almost flat dispersion along th Γ-X and Γ-Y directions over a range of crystal momentum, whose band top is in the vicinity of the Fermi level (E_F). From the E-k plot obtained with spin-orbit interactions [see right panel in Fig. 1(a)], we identify that the holelike and electronlike bands are split resulting in two sets of hole and electron pockets with slightly different sizes as shown in Fig. 1(b). There, we could find four electron pockets and four hole pockets. These calculations are in very good agreement with the calculations reported in Refs. [2,32], but are not consistent with the calculations reported in Ref. [33]. We further noticed that the number of electron pockets is sensitive to the position of E_F. A small increment of the Fermi level leads to the presence of several tiny electron pockets as reported in Ref. [2].

In Fig. 2 we show the ARPES data of $MoTe_2$ measured on sample A. In the Fermi surface map shown in Fig. 2(a), we can identify three well-connected—two jelly-bean-shaped

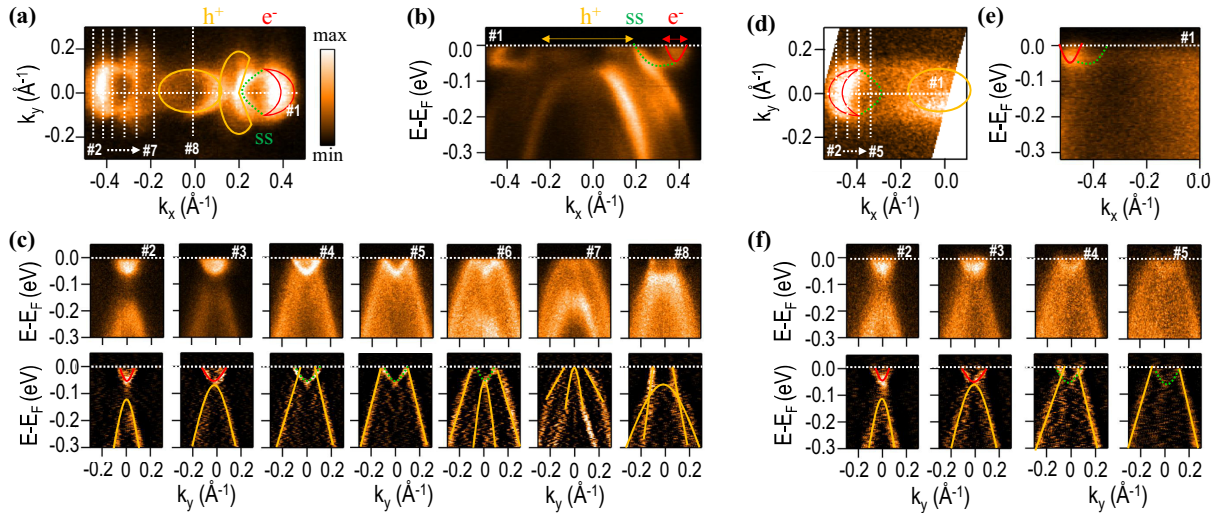

FIG. 2. ARPES data of $MoTe_2$ measured on sample A. All the data are measured using p-polarized light with a photon energy of $h\nu = 20$ eV. Note here that the 20 eV photon energy extracts the bands from the $k_z = 0$ plane [24,25]. The data shown in (a)–(c) are measured at a sample temperature of 20 K. (a) depicts the Fermi surface (FS) map. Solid curves represent bulk Fermi sheets, while the dashed curve represents Fermi arc from the surface. (b) shows energy the EDM taken along cut No. 1 as shown on the FS map. Top panels in (c) show EDMs taken along cuts No. 2 through No. 8 from left to right, respectively. Bottom panels in (c) are respective second derivatives of the EDMs shown in the top panels. (d)–(f) depict similar data of (a)–(c) except that these are measured at 130 K. On the FS maps the hole (yellow) and electron pockets (red) contributed from bulk are schematically shown by solid contours and the green dashed contours show the contribution from surface.

and one oval-shaped—hole pockets around the zone center (Γ) and two crescent-shaped electron pockets located along the k_x direction. It is also clear from the same map that the Fermi topology of these compounds is highly anisotropic; that means, the spectral intensity distribution along the k_x direction is entirely different from that along the k_y direction. This observation is in line with the anisotropy of crystal structure as well [see F. S1 in the Supplemental Material]. We further noticed an electronlike Fermi arc connecting both the bulk hole and electron pockets as shown by the green dashed curve in Fig. 2(a). This Fermi arc is ascribed to the presence of Weyl nodes in $MoTe_2$ [4,32]. The three hole pockets are related to the $h_3(h_4)$ Fermi sheet as shown in Fig. 1(b). We could not resolve the h_1 (h_2) hole pocket due to the matrix element effects.

To elucidate further the nature of electronlike and holelike band dispersions, we made cuts along the k_x and k_y directions as shown in Fig. 2(a). From Fig. 2(b), the energy distribution map (EDM) cut taken in the k_x direction, one can notice that the electronlike surface state disperses in such a way that it connects the bottom of the bulk electronlike band and the top of the bulk holelike band. As the band structure of these compounds is complex near the Fermi level it is difficult to disentangle the individual bands. From the EDM cuts taken in the k_y direction, we identified bulk electronlike band dispersion [see cuts No. 2 and No. 3 in Fig. 2(c)] and surface electronlike band dispersion [see cuts No. 4 through No. 6 in Fig. 2(c)]. Similarly, holelike bands are seen from cuts No. 7 and No. 8. These observations are consistent with the existing ARPES reports on $MoTe_2$ [23–28]. Figures 2(d)–2(f) depict similar data as shown in Figs. 2(a)–2(c) but measured at a sample temperature of 130 K. From Figs. 2(d)–2(f) it is clear that the band structure of $MoTe_2$ is largely intact with increase in temperature except that the bands are diffused due to thermal broadening. Nevertheless, due to this thermal broadening, we were unable to find the jelly-bean-shaped hole pockets from Fig. 2(d) which has relatively reduced spectral intensity in comparison to the other Fermi sheets [see Fig. 2(a)]. Nevertheless, the electronlike surface state is visible even at 130 K.

In Fig. 3 we show the ARPES data of $MoTe_2$ measured on sample B. Using the inner potential of 13 eV, we calculated that 45 eV photon energy extracts the bands from the $k_z = 0.1$ (π/c) plane. From the maps shown in the top panels of Fig. 3(a), we could identify one holelike Fermi sheet (oval-shaped) at the zone center and two electronlike Fermi sheets (crescent-shaped) on either side of the hole pocket located along the k_x direction. Surprisingly, we noticed two more oval-shaped Fermi sheets on either side of the hole pocket located at the Y points dispersing in the k_y direction. This Fermi sheet is not experimentally reported so far either from ARPES measurements [23–28] or from quantum oscillations [2] on $MoTe_2$, although it is found in our DFT calculations [see Fig. 1(a)] and as well in the reported DFT calculations [2,32]. To further elucidate the nature of these Fermi sheets, we made EDM cuts in the k_x and k_y directions as shown in the map [see Fig. 3(a)]. From cut No. 3 it is clear that the Fermi sheet shows electronlike band dispersion with a band bottom at $\approx$120 meV below E_F. The same is confirmed from the constant energy contours [see bottom panels in Fig. 3(a)] that the intensity of electron pockets at the Y point disappear

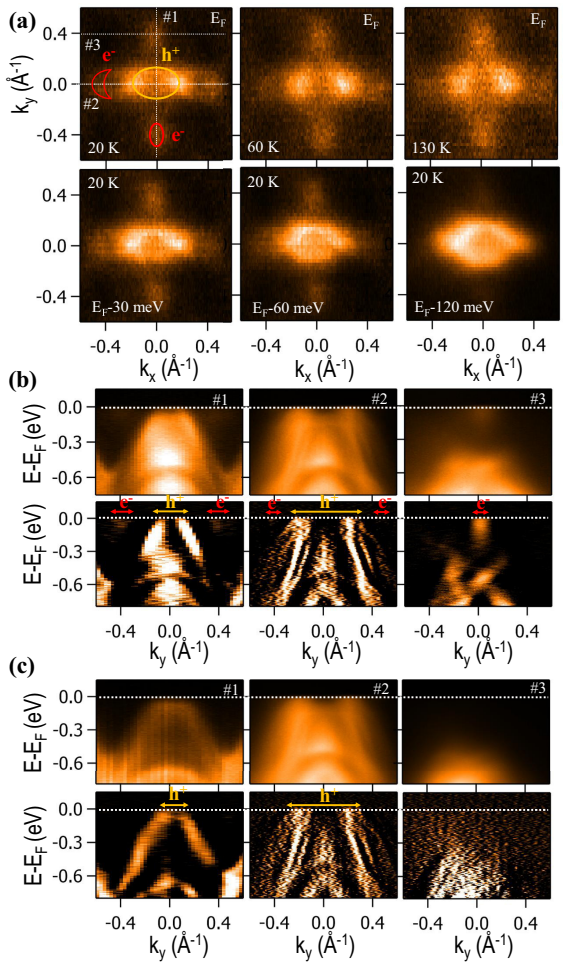

FIG. 3. ARPES data of $MoTe_2$ measured on sample B. All the data are measured with a photon energy of 45 eV. Top panels in (a) depict FS maps measured at sample temperatures of 20, 60, and 130 K. Bottom panels in (a) depict constant energy contours taken at binding energies $E_B = 30$, 60, and 120 meV at 20 K. In top panels of (b) we show EDMs taken along cuts No. 1 through No. 3 as shown on the FS map. Bottom panels of (b) are the second derivatives of respective EDMs shown in the top panels. (c) depicts similar data of (b) but measured with s-polarized light, while the data shown in (a) and (b) are measured with p-polarized light. Please see Fig. S2 given in the Supplemental Material for the definition of p- and s-polarized lights.

in the contour taken at a binding energy of 120 meV below E_F. We further examined that this electron pocket is absent when measured with s-polarized light [see Fig. 3(c)]. From cuts No. 1 and No. 2 we again found holelike band dispersions at the Γ point using both p-and s-polarized lights, consistent with the data of sample A. However, to emphasize, we found only one oval-shaped hole pocket from sample B, contrary to sample A in which we detected three hole pockets (two jelly-bean-shaped and one oval-shaped). Moreover, we did not find the electronlike surface state from the sample B. All this simply demonstrates that the cleavage plane of sample A is different from that of sample B (see also Fig. S2 in the Supplemental Material). This finding is consistent with the photoemission observations made on WTe_2 [34,35] where

it was shown that the differing cleavage planes lead to the differing band structures. The temperature-dependent data of the sample B are again consistent with sample A, i.e., the band structure of sample B is mostly intact with temperature when measured between 20 and 130 K. As can be seen from the top panels of Fig. 3(a), on increasing the sample temperature from 20 to 130 K, apart from trivial thermal broadening of the Fermi sheets we hardly detect any changes in the band structure. Further details on the orbital charter of these bands can be found in Fig. S3 in the Supplemental Material.

From the data taken on samples A and B, we found a momentum vector of 0.09 Å^{-1} for the crescent-shaped electron pocket in the k_y direction, momentum vectors of 0.13 and 0.07 Å^{-1} for the oval-shaped hole pocket in the k_x and k_y directions, respectively, and momentum vectors of 0.13 and 0.04 Å^{-1} for the jelly-bean-shaped hole pocket in the k_x and k_y directions, respectively. With the help of these momentum vectors and following the method shown in the Supplemental Material, we have calculated the number of electron (n_e) and hole (n_h) carriers, equivalent to 0.014 and 0.026 per unit cell, respectively. These values are estimated qualitatively without taking into account the k_z dependence of band structure and considering that the crescent-shaped electron and jelly-bean-shaped hole pockets are half-cylinder and half-elliptical cylinders, respectively, and the oval-shaped hole pocket is considered as an elliptical cylinder in three dimensions. Our estimate of $n_e = 0.014$/unit cell (4×10^{19} cm^{-3}) is in good agreement with the electron density values of 0.011/unit cell (2×10^{19} cm^{-3}) [2] and 0.0153/unit cell (5×10^{19} cm^{-3}) [33] reported on $MoTe_2$ at low temperatures using the quantum Hall measurements.

As reported here, the electronic structure of $MoTe_2$ is temperature independent in addition to the charge carrier imbalance. Therefore, the proposed theory of charge compensation for the nonsaturating XMR in these compounds seems to be invalid. A similar conclusion is arrived at in Ref. [36] using Hall probe, but lacked a quantitative analysis as we did here. In addition to the charge compensation, the other mechanisms are (i) magnetic field induced changes of the band structure [37], (ii) spin-orbit interaction [20,21], and (iii) nontrivial band topology with the time reversal symmetry breaking [38]. Point (iii) is not applicable to these semimetals as these ($MoTe_2$) show trivial band topology [25]. In the absence of magnetic field, it is highly unlikely that the spin-orbit interaction changes with temperature unless there is a structural transition which occurs only at 260 K. As can be seen in Fig. 1(a), one of the two holelike bands is flat up to a range of crystal momentum around the Γ point in the k_x and k_y directions, thus hinting at more localized hole pockets when compared to the electron pockets which are very dispersive near the Fermi level. This is in agreement with previous reports which showed that the electron carrier mobility (μ_e) is two times higher than the hole carrier mobility (μ_h) in $MoTe_2$ [2]. Hence, these compounds have dominant electron-type transport in $MoTe_2$ [2,33,39] although, as we showed above, the hole concentration is higher than the electron concentration. After ruling out point (iii) and charger carrier compensation as the mechanisms of nonsaturating XMR in $MoTe_2$, we suggest that the combination of Fermi surface deformation and spin-orbit interactions in the presence of external magnetic field could be a plausible mechanism. We also do not rule out a significant role played by the differing mobilities of holes and electrons [22].

In conclusion, we studied the low-energy band structure of $MoTe_2$ semimetal by means of an ARPES technique and DFT calculations. The ARPES data on two different samples from the same preparation batch demonstrate that the band structure is cleavage dependent, similar to what was recently observed in WTe_2 [34]. Overall, the experimental findings are quantitatively consistent with our DFT calculations. Our results further demonstrate that $MoTe_2$ is a noncompensated semimetal as we found qualitatively that the number of hole carriers (n_h) is higher than electron carriers (n_e). This observation invalidates the theory of charge compensation for the nonsaturating XMR in $MoTe_2$. The temperature-independent band structure of $MoTe_2$ adds further difficulties in understanding the temperature-dependent XMR recorded in $MoTe_2$. We believe our results of $MoTe_2$ present invaluable information to the emerging field of XMR physics in type-II Weyl semimetals and suggest a revision on the current understanding of the nonsaturating XMR of these compounds.

ACKNOWLEDGMENTS

S.T. acknowledges support by the Department of Science and Technology, India through the INSPIRE-Faculty program (Grant No. IFA14 PH-86). The authors thank the Department of Science and Technology, India (SR/NM/Z-07/2015) for the financial support and Jawaharlal Nehru Centre for Advanced Scientific Research (JNCASR) for managing the project. The authors acknowledge the financial support given for the measurements at Elettra Synchrotron under Indo-Italian (DST-ICTP) Cooperation Program. R.A.R. acknowledges support by FAPESP (Grant No. 2011/19924-2). This work has been partly performed in the framework of the Nanoscience Foundry and Fine Analysis (NFFA-MIUR Italy) project.

[1] M. N. Ali, J. Xiong, S. Flynn, J. Tao, Q. D. Gibson, L. M. Schoop, T. Liang, N. Haldolaarachchige, M. Hirschberger, N. P. Ong, and R. J. Cava, Large, Non-saturating magnetoresistance in WTe_2, Nature (London) **514**, 205 (2014).

[2] Q. Zhou, D. Rhodes, Q. R. Zhang, S. Tang, R. Schönemann, and L. Balicas, Hall effect within the colossal magnetoresistive semimetallic state of $MoTe_2$, Phys. Rev. B **94**, 121101 (2016).

[3] A. A. Soluyanov, D. Gresch, Z. Wang, Q. Wu, M. Troyer, X. Dai, and B. Andrei Bernevig, Type-II Weyl semimetals, Nature (London) **527**, 495 (2015).

[4] Y. Sun, S.-C. Wu, M. N. Ali, C. Felser, and B. Yan, Prediction of Weyl semimetal in orthorhombic $MoTe_2$, Phys. Rev. B **92**, 161107 (2015).

[5] M. N. Baibich, J. M. Broto, A. Fert, F. Nguyen Van Dau, F. Petroff, P. Etienne, G. Creuzet, A. Friederich, and J. Chazelas,

Giant Magnetoresistance of (001)Fe/(001)Cr Magnetic Superlattices, Phys. Rev. Lett. **61**, 2472 (1988).

[6] G. Binasch, P. Grünberg, F. Saurenbach, and W. Zinn, Enhanced magnetoresistance in layered magnetic structures with antiferromagnetic interlayer exchange, Phys. Rev. B **39**, 4828 (1989).

[7] M. B. Salamon and M. Jaime, The physics of manganites: Structure and transport, Rev. Mod. Phys. **73**, 583 (2001).

[8] L. Schubnikow and W. J. De Haas, A new phenomenon in the change of resistance in a magnetic field of single crystals of bismuth. Nature (London) **126**, 500 (1930).

[9] R. Xu, A. Husmann, T. F. Rosenbaum, M. L. Saboungi, J. E. Enderby, and P. B. Littlewood, Large magnetoresistance in non-magnetic silver chalcogenides, Nature (London) **390**, 57 (1997).

[10] F. Y. Yang, Large magnetoresistance of electrodeposited single-crystal bismuth thin films, Science **284**, 1335 (1999).

[11] M. Lee, T. F. Rosenbaum, M.-L. Saboungi, and H. S. Schnyders, Band-Gap Tuning and Linear Magnetoresistance in the Silver Chalcogenides, Phys. Rev. Lett. **88**, 066602 (2002).

[12] R. S. Singh, X. Wang, W. Chen, Ariando, and A. T. S. Wee, Large room-temperature quantum linear magnetoresistance in multilayered epitaxial graphene: Evidence for two-dimensional magnetotransport, Appl. Phys. Lett. **101**, 183105 (2012).

[13] D.-X. Qu, Y. S. Hor, J. Xiong, R. J. Cava, and N. P. Ong, Quantum oscillations and Hall anomaly of surface states in the topological insulator Bi_2Te_3, Science **329**, 821 (2010).

[14] X. Wang, Y. Du, S. Dou, and C. Zhang, Room Temperature Giant and Linear Magnetoresistance in Topological Insulator Bi_2Te_3 Nanosheets, Phys. Rev. Lett. **108**, 266806 (2012).

[15] T. Liang, Q. Gibson, M. N. Ali, M. Liu, R. J. Cava, and N. P. Ong, Ultrahigh mobility and giant magnetoresistance in the Dirac semimetal Cd_3As_2, Nat. Mater. **14**, 280 (2014).

[16] J. Feng, Y. Pang, D. Wu, Z. Wang, H. Weng, J. Li, X. Dai, Z. Fang, Y. Shi, and L. Lu, Large linear magnetoresistance in Dirac semimetal Cd_3As_2 with Fermi surfaces close to the Dirac points, Phys. Rev. B **92**, 081306 (2015).

[17] L.-K. Zeng, R. Lou, D.-S. Wu, Q. N. Xu, P.-J. Guo, L.-Y. Kong, Y.-G. Zhong, J.-Z. Ma, B.-B. Fu, P. Richard *et al.*, Compensated Semimetal LaSb with Unsaturated Magnetoresistance, Phys. Rev. Lett. **117**, 127204 (2016).

[18] Y.-Y. Lv, B.-B. Zhang, X. Li, S.-H. Yao, Y. B. Chen, J. Zhou, S.-T. Zhang, M.-H. Lu, and Y.-F. Chen, Extremely large and significantly anisotropic magnetoresistance in ZrSiS single crystals, Appl. Phys. Lett. **108**, 244101 (2016).

[19] I. Pletikosić, M. N. Ali, A. V. Fedorov, R. J. Cava, and T. Valla, Electronic Structure Basis for the Extraordinary Magnetoresistance in WTe_2, Phys. Rev. Lett. **113**, 216601 (2014).

[20] J. Jiang, F. Tang, X. C. Pan, H. M. Liu, X. H. Niu, Y. X. Wang, D. F. Xu, H. F. Yang, B. P. Xie, F. Q. Song, P. Dudin, T. K. Kim, M. Hoesch, P. K. Das, I. Vobornik, X. G. Wan, and D. L. Feng, Signature of Strong Spin-Orbital Coupling in the Large Nonsaturating Magnetoresistance Material WTe_2, Phys. Rev. Lett. **115**, 166601 (2015).

[21] P. Kumar Das, D. Di Sante, I. Vobornik, J. Fujii, T. Okuda, E. Bruyer, A. Gyenis, B. E. Feldman, J. Tao, R. Ciancio, G. Rossi, M. N. Ali, S. Picozzi, A. Yadzani, G. Panaccione, and R. J. Cava, Layer-dependent quantum cooperation of electron and hole states in the anomalous semimetal WTe_2, Nat. Commun. **7**, 10847 (2016).

[22] J. He, C. Zhang, N. J. Ghimire, T. Liang, C. Jia, J. Jiang, S. Tang, S. Chen, Y. He, S.-K. Mo, C. C. Hwang, M. Hashimoto, D. H. Lu, B. Moritz, T. P. Devereaux, Y. L. Chen, J. F. Mitchell, and Z.-X. Shen, Distinct Electronic Structure for the Extreme Magnetoresistance in YSb, Phys. Rev. Lett. **117**, 267201 (2016).

[23] J. Jiang, Z. K. Liu, Y. Sun, H. F. Yang, C. R. Rajamathi, Y. P. Qi, L. X. Yang, C. Chen, H. Peng, C-C. Hwang, S. Z. Sun, S-K. Mo, I. Vobornik, J. Fujii, S. S. P. Parkin, C. Felser, B. H. Yan, and Y. L. Chen, Signature of type-II Weyl semimetal phase in $MoTe_2$, Nat. Commun. **8**, 13973 (2017).

[24] N. Xu, Z. J. Wang, A. P. Weber, A. Magrez, P. Bugnon, H. Berger, C. E. Matt, J. Z. Ma, B. B. Fu, B. Q. Lv, N. C. Plumb, M. Radovic, E. Pomjakushina, K. Conder, T. Qian, J. H. Dil, J. Mesot, H. Ding, and M. Shi, Discovery of Weyl semimetal state violating Lorentz invariance in $MoTe_2$, arXiv:1604.02116.

[25] A. Tamai, Q. S. Wu, I. Cucchi, F. Y. Bruno, S. Riccò, T. K. Kim, M. Hoesch, C. Barreteau, E. Giannini, C. Besnard, A. A. Soluyanov, and F. Baumberger, Fermi Arcs and Their Topological Character in the Candidate Type-II Weyl Semimetal $MoTe_2$, Phys. Rev. X **6**, 031021 (2016).

[26] K. Deng, G. Wan, P. Deng, K. Zhang, S. Ding, E. Wang, M. Yan, H. Huang, H. Zhang, Z. Xu, J. Denlinger, A. Fedorov, H. Yang, W. Duan, H. Yao, Y. Wu, S. Fan, H. Zhang, X. Chen, and S. Zhou, Experimental observation of topological Fermi arcs in type-II Weyl semimetal $MoTe_2$, Nat. Phys. **12**, 1105 (2016).

[27] L. Huang, T. M. McCormick, M. Ochi, Z. Zhao, Michi-To Suzuki, R. Arita, Y. Wu, D. Mou, H. Cao, J. Yan, N. Trivedi, and A. Kaminski, Spectroscopic evidence for a type-II Weyl semimetallic state in $MoTe_2$, Nat. Mater. **15**, 1155 (2016).

[28] A. Liang, J. Huang, S. Nie, Y. Ding, Q. Gao, C. Hu, S. He, Y. Zhang, C. Wang, B. Shen *et al.*, Electronic evidence for type II Weyl semimetal state in $MoTe_2$, arXiv:1604.01706.

[29] A. Crepaldi, G. Autès, A. Sterzi, G. Manzoni, M. Zacchigna, F. Cilento, I. Vobornik, J. Fujii, Ph. Bugnon, A. Magrez, H. Berger, F. Parmigiani, O. V. Yazyev, and M. Grioni, Persistence of a surface state arc in the topologically trivial phase of $MoTe_2$, Phys. Rev. B **95**, 041408(R) (2017).

[30] See Supplemental Material at http://link.aps.org/supplemental/10.1103/PhysRevB.95.241105 for the details on carrier density estimate, crystal structure information and for the additional data from ARPES and DFT calculations on $MoTe_2$.

[31] Band structure calculations are performed on the orthorhombic crystal structure of $MoTe_2$ [33] having the lattice constants $a = 3.477$ Å, $b = 6.335$ Å, and $c = 13.889$ Å using density functional theory (DFT) within the generalized gradient approximation (GGA) of Perdew, Burke, and Ernzerhof (PBE) exchange and correlation potential [40] as implemented in the Quantum Espresso simulation package [41]. Norm conserving scalar relativistic and fully relativistic pseudopotentials are used to perform calculations without spin-orbit coupling (SOC) and with SOC, respectively. The electronic wave function is expanded using plane waves up to a cutoff energy of 50 Ry (680 eV). Brillouin zone sampling is done over a $(24 \times 14 \times 6)$ Monkhorst-Pack-k grid. During the calculation we have fixed the experimentally obtained lattice parameters and atomic positions to compare with the band structure from ARPES studies.

[32] Z. Wang, D. Gresch, A. A. Soluyanov, W. Xie, S. Kushwaha, X. Dai, M. Troyer, R. J. Cava, and B. A. Bernevig, $MoTe_2$: A Type-II Weyl Topological Metal, Phys. Rev. Lett. **117**, 056805 (2016).

[33] Y. Qi, P. G. Naumov, M. N. Ali, C. R. Rajamathi, W. Schnelle, O. Barkalov, M. Hanfland, S.-C. Wu, C. Shekhar, Y. Sun *et al.*, Superconductivity in Weyl semimetal candidate $MoTe_2$, Nat. Commun. **7**, 11038 (2016).

[34] Y. Wu, D. Mou, N. H. Jo, K. Sun, L. Huang, S. L. Bud'ko, P. C. Canfield, and A. Kaminski, Observation of Fermi arcs in the type-II Weyl semimetal candidate WTe_2, Phys. Rev. B **94**, 121113(R) (2016).

[35] F. Y. Bruno, A. Tamai, Q. S. Wu, I. Cucchi, C. Barreteau, A. de la Torre, S. McKeown Walker, S. Riccò, Z. Wang, T. K. Kim, M. Hoesch, M. Shi, N. C. Plumb, E. Giannini, A. A. Soluyanov, and F. Baumberger, Observation of large topologically trivial Fermi arcs in the candidate type-II Weyl semimetal WTe_2, Phys. Rev. B **94**, 121112(R) (2016).

[36] T. Zandt, H. Dwelk, C. Janowitz, and R. Manzke, Quadratic temperature dependence up to 50 K of the resistivity of metallic, J. Alloys Compd. **442**, 216 (2007).

[37] K. Wang, D. Graf, L. Li, L. Wang, and C. Petrovic, Anisotropic giant magnetoresistance in $NbSb_2$, Sci. Rep. **4**, 7328 (2014).

[38] F. F. Tafti, Q. D. Gibson, S. K. Kushwaha, N. Haldolaarachchige, and R. J. Cava, Resistivity plateau and extreme magnetoresistance in LaSb, Nat. Phys. **12**, 272 (2015).

[39] D. H. Keum, S. Cho, J. H. Kim, D.-H. Choe, H.-J. Sung, M. Kan, H. Kang, J.-Y. Hwang, S. W. Kim, H. Yang, K. J. Chang, and Y. H. Lee, Bandgap opening in few-layered monoclinic $MoTe_2$, Nat. Phys. **11**, 482 (2015).

[40] J. P. Perdew, K. Burke, and M. Ernzerhof, Generalized Gradient Approximation Made Simple, Phys. Rev. Lett. **77**, 3865 (1996).

[41] P. Giannozzi, S. Baroni, N. Bonini, M. Calandra, R. Car, C. Cavazzoni, D. Ceresoli, G. L. Chiarotti, M. Cococcioni, I. Dabo *et al.*, QUANTUM ESPRESSO: A modular and open-source software project for qQuantum simulations of materials, J. Phys.: Condens. Matter **21**, 395502 (2009).